

NUMERICAL AND ANALYTICAL MODEL OF INDUCTION MOTOR FOR COMPUTER AIDED DESIGN

Vasilija Sarac¹, Dragan Minovski¹, Peter Janiga²

¹ Faculty of Electrical Engineering, University "Goce Delcev", P.O.Box 201,
2000 Stip

² Faculty of Electrical Engineering and Information Technology, Slovak University
of Technology in Bratislava, Ilkovičova 3, 81219 Bratislava
e-mails: vasilija.sarac@ugd.edu.mk, dragan.minovski@ugd.edu.mk, pe-
ter.janiga@stuba.sk

¹ R. Macedonia, ² R. Slovakia

Abstract: Paper presents analytical and numerical model of three-phase asynchronous squirrel cage motor suitable for fast computation of motor steady state and transient performance characteristics at various operating modes: no-load, rated load and locked rotor. From the motor analytical model, numerical model for computing transient characteristics and magnetic flux density in motor cross-section is deduced. Accuracy of the analytical model is verified by experiment. Influence of various design parameters on motor torque is studied. Derived computer models allow fast changes in motor design and development of various motor variants with improved performance characteristics.

Key words: induction motor, finite element method, transient characteristics, steady-state characteristics.

1. INTRODUCTION

Electrical machines are used in more and novel application throughout the world, driven by the need for greater power efficiency in the transportation, aerospace, defense, and industrial automation markets. There is a clear global demand to develop more power-efficient machines but progress has been hindered due to the large amount of computation resources and time required to simulate an electrical machines. This issue becomes especially important in case of electromagnetic fields simulation inside the electrical machines. It is a huge computational undertaking to characterize an electrical machine of any kind for steady-state operation. This limits the number of design points that engineers can acquire in a reasonable amount of time to make critical design decisions [1]. Design of the three-phase induction squir-

rel cage motor, belongs to the well-known designs of the induction motors, which involves calculation of motor parameters such as: reactance and inductances, as well as motor performance characteristics of torque, currents, efficiency, power factor and output power at different speeds [2-6]. Paper proposes the analytical model suitable for fast computation of three phase induction motor parameters and steady-state performance characteristics. The model requires several input parameters related to the motor geometry and laminations of the stator and the rotor. As an output from the analytical model all important motor parameters are calculated as well as the steady-state performance characteristics with computation time of several seconds [7]. The motor design can be simply altered by varying some of the input design parameters such as motor length, input voltage, stator diameter or stator winding parameters. On that way, several design alternatives can be created quickly with short computational time and the designer can decide which model is the best for a given application. The results from the analytical model are compared with the experimental data for validation of model accuracy. Analytical model of the motor does not provide data of magnetic flux density distribution in motor cross-section i.e. the parts of magnetic core with high saturation and losses cannot be detected only by the analytical model. In recent years, different numerical techniques have been developed for simulation of low frequency electromagnetic fields based on several approaches: finite differences, finite elements and finite volumes [8-15]. The finite element method (FEM) is widely used in engineering practice because it can model complex inhomogeneous, anisotropic materials and represent complicated geometry using irregular grids. Paper proposes three different numerical models based on FEM for three different operating modes: no-load, rated load and locked rotor. Transient characteristics of torque and currents are obtained from the numerical models. They allow understanding of different operating modes of the motor during motor acceleration and steady-state operation. Finally, influence of several design parameters on motor torque is analyzed, by applying the parametric analysis in motor numerical model. The latest analysis allows the designer to make several motor designs in very short time, to understand the influence of various design parameters on motor performance and finally to choose the best design for the given application.

2. ANALYSIS APPROACH FOR THREE-PHASE INDUCTION MOTOR

2.1. Analytical model

For a three-phase induction motor, the stator winding (with a sinusoidal spatial distribution and p pairs of poles) is connected to a three-phase symmetric voltage power supply. The resulting currents in the stator winding produce a rotating magnetic field. The rotor winding is often a squirrel cage type. Currents are induced in the rotor bars and produce, in turn, a second rotating magnetic field. The two rotat-

ing fields produce a resultant rotating magnetic field in the air gap of the machine. The interaction of this field in the air gap with the rotor bar currents produces an electromagnetic torque, which acts on the rotor in the direction of the rotation of the field in the air gap [7]. The performance of three-phase induction motors is analyzed based on the equivalent circuit of one phase in the frequency domain as shown in Fig. 1.

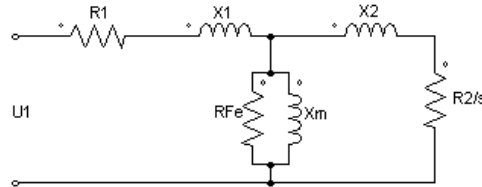


Figure 1. Induction motor equivalent circuit

In the Fig. 1, R_1 is the stator resistance, X_1 is stator leakage reactance, which consists of stator slot leakage reactance, end-winding leakage reactance, and differential leakage reactance. X_2 and R_2 are rotor leakage reactance and rotor resistance, respectively. X_2 includes rotor slot leakage reactance, end-ring leakage reactance, differential leakage reactance, and skewing leakage reactance. The parameters in the equivalent circuit are dependent on the stator and rotor currents. Rotor parameters vary with the rotor slip- s . All rotor parameters have been referred to the stator side. X_m is the magnetizing reactance, and R_{Fe} is the resistance corresponding to iron-core losses. X_m is a linearized nonlinear parameter that varies with the saturation of the main field. The electromagnetic power P_m , or air-gap power, is computed by the following:

$$P_m = 3 \cdot I_2^2 \cdot R_2 / s \tag{1}$$

I_2 is the rotor current calculated from the transformation of the equivalent circuit from Fig. 1.

Electromagnetic torque is:

$$T_m = P_m / \omega \tag{2}$$

where ω is synchronous speed in rad/s. The output mechanical torque T_2 is:

$$T_2 = T_m - T_{fw} \tag{3}$$

T_{fw} is the frictional and wind torque.

The output power is:

$$P_2 = T_2 \cdot \omega_2 \tag{4}$$

where $\omega_2 = \omega(1-s)$ is the rotor speed in rad/s as s is the motor slip.

The input power is:

$$P_1 = P_2 + P_{cu2} + P_{Fe} + P_{cu1} + P_s \tag{5}$$

P_{cu2} , P_{Fe} , P_{cu1} and P_s are rotor copper loss, iron-core loss, stator copper loss and stray loss respectively.

The power factor is derived from :

$$\cos \varphi = P_1 / m \cdot U_1 \cdot I_1 \quad (6)$$

m is the number of phases The efficiency is computed by:

$$\eta = \frac{P_2}{P_1} \cdot 100 \quad (7)$$

Stator resistance is found from:

$$R_1 = \rho_{cu} \cdot \frac{l_c W_1}{A_{co} a_1} \quad (8)$$

ρ_{cu} is the resistance of copper, l_c is the coil length including active part of the winding and end connections, W_1 is the number of turns in stator winding, A_{co} is the conductor cross-section and a_1 is the number of current paths in parallel.

Rotor resistance- R_2 is consisted of the rotor bar resistance and end ring resistance.

$$R_2 = k_2 (R_b + R_r) \quad (9)$$

R_b is the rotor bar resistance and R_r is the end ring resistance. k_2 is the coefficient for referring the rotor resistance to stator winding.

Rotor bar resistance is:

$$R_b = \rho_{al} \cdot \frac{l}{S_b} \quad (10)$$

ρ_{al} is the resistance of the aluminum as rotor cage winding is from aluminum, l is the bar length and S_b is the bar cross-section. Ring resistance is found from:

$$R_r = 2\pi D_r \rho_{al} / Z_2 S_r k_r^2 \quad (11)$$

D_r is the average ring diameter, Z_2 number of rotor slots, S_r -ring cross section and k_r coefficient of refereeing the ring current to bar current.

Stator leakage reactance is calculated from:

$$X_1 = 1.58 f_1 l_1 W_1^2 \lambda_1 / (p q_1 10^8) \quad (12)$$

f_1 -supply frequency, l_1 -motor length, λ_1 -leakage coefficient of stator winding, q_1 -number of stator slots per phase per pole.

Rotor leakage reactance is calculated from:

$$X_2 = k_2 \cdot (7.9 f_1 l_1 \lambda_2 10^{-9}) \quad (13)$$

λ_2 is the leakage coefficient of rotor winding. Magnetizing reactance is calculated from:

$$X_m = E / I_m \quad (14)$$

where E is the induced voltage and I_m is the magnetizing current.

$$I_m = 2.22 F_{sum} p / (m W_1 k_w) \quad (15)$$

F_{sum} is the sum of magnetomotive forces per pole and k_w is the winding coefficient.

2.2. Experiments

Experiments are performed on motor type 2AZ 155-4 from company Rade Koncar. Rated data obtained from the motor producer are: output power P_2 of 2.2 kW, line current at 220 V in delta winding connection of 8,7 A, or at 380 V and star connection of stator winding phase/line current of 5 A, power factor $\cos\varphi$ of 0.81 and rated speed 1410 rpm. The newer version of the same motor is presented in Koncar catalog as motor type 5AZ 100LA-4 [16]. The purpose of the experiments is to determine the main motor operating characteristics such as input power P_1 , output power P_2 , output torque M_2 , power factor $\cos\varphi$, efficiency factor η and to compare them, first with manufacturer data and second with the results obtained from computer model of the motor for calculating steady-state characteristics. Motor is connected to the power supply according to Fig. 2.

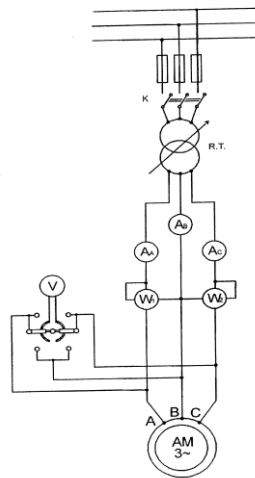


Figure 2. Measuring circuit

At rated voltage motor is loaded up to the value of rated current while motor voltage is kept constant 220 V. Voltmeter, ammeter and wattmeter are read out. On that way, motor input power is measured from:

$$P_1 = k_w(\alpha_1 \pm \alpha_2) \quad (16)$$

k_w - wattmeter constant W/no. of scale parts, α_1 and α_2 number of parts of the scale of the wattmeter from reading of the instrument.

Output power is:

$$P_2 = P_1 - (P_k + P_{Fe} + P_s) \quad (17)$$

P_k are the short circuit losses, i.e.

$$P_k = P_{cu1} + P_{cu2} \quad (18)$$

Short circuit losses are found from the locked rotor experiment (rotor of the machines is in stand-still while the stator current is gradually increased up to the rated current and simultaneously voltage is measured- U_{lk}). Iron losses- P_{Fe} and stray losses- P_s are obtained from the no-load experiment (motor is accelerated without load up to the rated voltage of 220 V). In that case, iron and stray losses are equal to:

$$P_{Fe} + P_s = P_0 - 3R_1 I_0^2 \quad (19)$$

P_0 is the input power of the motor at no load from wattmeter readings, I_0 is the measured stator winding current at no-load from ammeters readings, and R_1 is the measured resistance with ohmmeter. The sum of iron and stray losses at rated voltage 220 V is 147.99 W.

On the base of measurements output torque- T_2 , power factor- $\cos\varphi$ and efficiency- η factor are calculated respectively:

$$T_2 = 9.55 \frac{P_2}{n} \quad (20)$$

n – rotor speed in rpm/min and P_2 is the motor output power in watts.

$$\cos\varphi = \frac{P_1}{\sqrt{3}U_{ll}I_{ll}} \quad (21)$$

U_{ll} , I_{ll} –measured line voltage and currents

$$\eta = \frac{P_2}{P_1} \quad (22)$$

Results from measurements of a loaded motor are presented in Table 1.

Table 1. Motor measurements

Locked rotor		No-load	Loaded motor							
U_{lk} (V)	P_k (W)	$P_{Fe\&P_s}$ (W)	U_{ll} (V)	I_{ll} (A)	n (rpm)	P_1 (W)	P_2 (W)	T_2 (Nm)	$\cos\varphi$ (/)	η (/)
48.62	417	147.9	220	8.44	1410	2510	1945	13.17	0.78	0.775
43	325	147.9	220	7.45	1430	2290	1817	12.1	0.80	0.793
38.3	284.6	147.9	220	6.57	1440	1910	1477	9.79	0.76	0.777
32.75	242.3	147.9	220	5.63	1450	1440	1049.7	6.91	0.67	0.728
30.17	225	147.9	220	5.23	1455	1270	897.01	5.88	0.63	0.706
26.1	192.3	147.9	220	4.48	1470	790	449.7	2.92	0.46	0.569
24.8	180.8	147.9	220	4.2	1475	430	101.2	0.655	0.26	0.236

3. COMPUTER AIDED DESIGN OF ANALYTICAL AND NUMERICAL MODEL

Next step in the motor analysis is to build the model of the motor in software Maxwell suitable for calculating motor steady-state characteristics. All motor data necessary for the motor design and performance analysis are presented in Table 2. Based on the data from the producer, stator and rotor laminations are input into computer model of the motor (Fig. 3a). Next step in modelling the motor analytical model is to calculate and design the stator winding (Fig. 3b). Stator winding is a three-phase distributed winding and its parameters are presented in Table 3. Rotor winding is an aluminium cage winding with parameters presented in Table 4. Once, the all motor parameters (stator and rotor laminations, motor axial length, rated parameters and materials properties) are input, analytical model of the motor in software program Maxwell, is ready for calculating the steady – state characteristics.

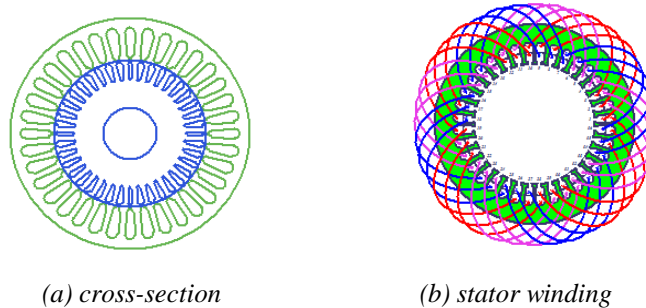


Figure 3. Modelling motor cross-section and stator winding

Table 2. Motor data

<i>nominal power</i>	$P=2.2 \text{ kW}$
<i>number of poles</i>	$2p=4$
<i>nominal voltage Δ/Y</i>	$220/380 \text{ V}$
<i>nominal current Δ/Y</i>	$8.7/5 \text{ A}$
<i>power factor</i>	$\cos\varphi=0.81$
<i>nominal speed</i>	1410 rpm
<i>number of stator slots</i>	$Z_1=36$
<i>number of rotor slots</i>	$Z_2=40$
<i>stator winding resistance per phase</i>	$R_1=2.76 \ \Omega$
<i>stator outer diameter</i>	$D_{sa}=152 \text{ mm}$
<i>stator inner diameter</i>	$D_{si}=97 \text{ mm}$
<i>radial air gap length</i>	$g=0.6 \text{ mm}$
<i>stack length</i>	$l_{FE}=100$
<i>nominal frequency</i>	$f=50 \text{ Hz}$

Table 3. Stator winding data

winding layers	2
parallel branches	2
conductor per slot	$N_c=97$
coil pitch	7

Table 4. Rotor winding data

IM bar conductor	cast aluminium
IM end ring width	8 mm
IM end ring height	19 mm

As an output from software program, the motor steady-state characteristics of stator winding current (I_1), efficiency factor (η), power factor ($\cos\phi$), output power (P_2) and torque (T_2) for different speeds (n) are calculated. Calculation of the steady-state characteristics is closely related to calculation of motor parameters and they are obtained as an output from the analytical model of the motor in Maxwell software. Based on motor model for computer aided design and calculation of steady-state characteristics the numerical model of the motor is derived. Numerical model uses FEM for simulation of transient low-frequency electromagnetic fields. Transient electromagnetic field simulation allows analysis of dynamic systems with nonlinear materials and permanent magnets under a variety of conditions, employing sinusoidal waveforms and particularly any other pulsed wave excitations. The process requires sequential calculation, over many time steps, of saturation, eddy currents, slotting effects and rotor movement in time and space [1]. The procedure of transient simulations includes discretization of whole domain of analyzed object, in this case the motor, into numerous elements (usually triangles) that create the mesh of finite elements (Fig. 4).

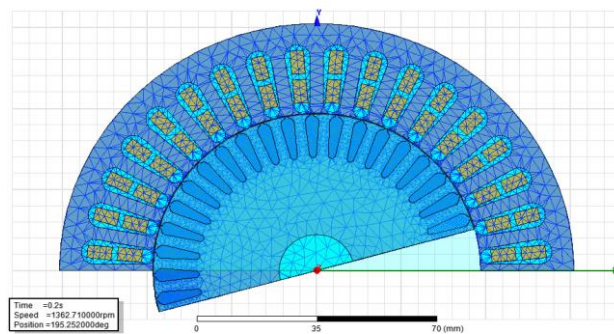


Figure 4. Mesh of finite elements in motor cross-section

For each element magnetic vector potential \mathbf{A} is found and from \mathbf{A} , the vector of magnetic flux density \mathbf{B} is deduced. The problem is solved for sinusoidal excitation

with frequency of 50 Hz. FEM is used to solve the Maxwell set of equations. FEM discretization produces a set of matrix differential equations. They are solved with time decomposition method (TDM). The domain is decomposed along time axis and all time steps are solved simultaneously instead of solving them time step by time step. The nonlinear matrix equations are linearized for each of the nonlinear iterations. As an output results from the numerical models the magnetic flux density in motor cross-section is plotted and the transient characteristics of torque and currents for different operating modes- no load, rated load and locked rotor are obtained as well.

In the numerical model parametric analysis is run with respect to several design possibilities of two parameters: stator inner diameter (length of the air gap) and stator voltage. The variations of these two parameters are presented in Table 5.

Table 5. Ranges of variations of design parameters

<i>Parameter</i>	<i>Variation range</i>
Stator inner diameter	(97-97.4) mm
Stator voltage –amplitude	(300-315) V

It should be stated that parametric analysis is run for end values of each parameter, i.e. stator inner diameter 97 mm or 97.4 mm and the amplitude of the stator voltage 300 or 315 V. On that way, four design alternatives are created. Each of the alternatives is analyzed with respect to its influence on motor torque. Motor basic model is for voltage 310 V and stator inner diameter of 97 mm. Parametric analysis is run at rated load operation.

4. RESULTS AND DISCUSSIONS

Analytical model of three-phase induction motor in Maxwell software allows calculation of parameters and steady-state characteristics of the motor. Steady-state characteristics of stator current, efficiency, output power, power factor and torque for different speeds are presented in Fig .5. They are computed for different motor speeds, i.e. slips, allowing insight into the complete motor operating range from slip zero to one.

Accuracy of the motor analytical model is verified by comparing the basic output results of this model with data from the motor producer based on experiments in its premises and experiments in faculty laboratory. This comparison is presented in Table 6.

Producer of the motor declares in star connection of stator winding and supply voltage of 380 V stator-winding current of 5A [16]. According to the Fig. 5a at speed of 1362 rpm which is the rated speed from the analytical model and supply voltage of 380 V, the current is 5.1 A.

Table 6. Comparison of analytical model and measurements

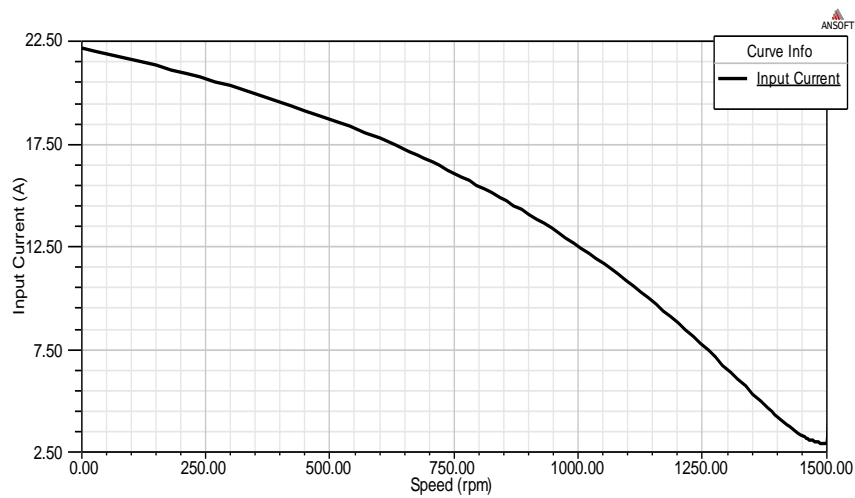
	Analytical model	Producer data	Measurements
<i>Star connection, voltage 380 V</i>			
<i>rated phase current (A)</i>	5.1	5	4.87
<i>no-load phase current (A)</i>	2.9	2.4	2.36
<i>no-load input power (W)</i>	142	170	196
<i>locked-rotor phase current (A)</i>	22.1	25	/
<i>nominal output power (kW)</i>	2.12	2.2	1.94
<i>nominal power factor</i>	0.8	0.81	0.78
<i>rated speed (rpm)</i>	1362	1410	1410
<i>rated torque (Nm)</i>	15	14.9	13.17

In the measurements (Table 1) according to the average value from three ammeter in all three phases the line current for 220 V and delta connection at 1410 rpm is 8.44A or this gives the phase current of 4.87 A. No load current according to Fig. 5a at speed of 1490 rpm is 2.9 A, according to the measurement at 220 V, the line current is 4.1 A or phase current of 2.36 A. For the no-load operation at 1490 rpm Fig. 5c gives an output power of 142 W. From the measurements at no-load at 1490 rpm the output power is 196 W. The producer specifies the no-load power 170 W. Locked rotor current or short circuit current is compared only with the producer data, which is 25 A [16]. Locked rotor current is measured only up to the value of rated current at decreased supply voltage in order not to damage the machine by the short circuit current. Locked rotor current in analytical model is obtained from Fig. 5a at zero speed and it is 22.1 A. Value of nominal output power from Fig 5c at 1366 rpm (since 1366 rpm is the nominal speed of the analytical model) is 2.12 kW. This value is compared with the result from Table 1 at 1410 rpm the rated output power P_2 is 1.94 kW. The motor producer declares rated output power of 2.2 kW [16]. From Fig. 5d, power factor at 1362 rpm (rated speed of analytical model) is 0.8, while from measurements in Table 1 at 1410 rpm (rated speed of the machine in experiments) it is 0.78. Producer declares power factor of 0.81 [16]. Analytical model calculates the rated operating point at speed 1362 rpm while the producer and measurement set the operating point (speed at which rated power and torque are obtained) at 1410 rpm. Rated torque from analytical model is obtained at 1362 rpm at Fig. 5e and its value is 15 Nm. Torque of the producer is easily found using the equation (20). The producer declares rated power P_2 of 2.2 kW and rated speed n of 1410 rpm, which give the output torque of 14.9 Nm. Value of the torque from measurements is somewhat lower 13.7 Nm (Table 1), but still sufficiently close to

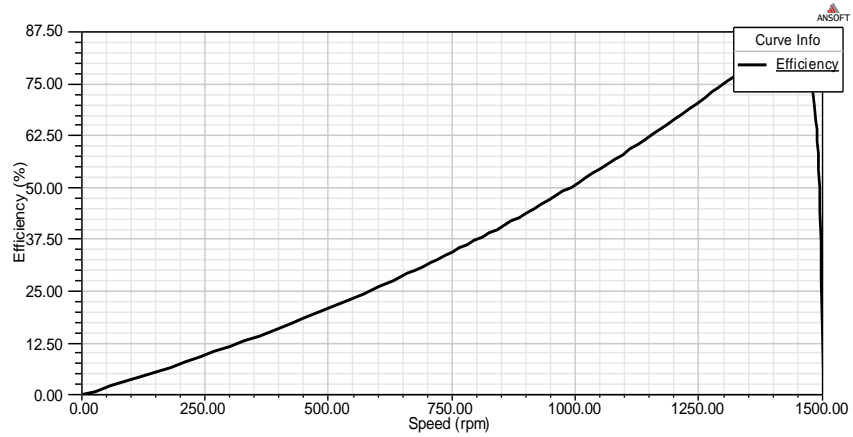
the value from producer data and analytical model. Results presented in Table 6 verify the accuracy of analytical model as obtained data from this model are very close to the measurements. Analytical model is calculated for constant torque application. Therefore, the output torque from the analytical model and producer data are almost identical that verifies the model as accurate enough. From previous analysis of steady-state characteristics and their comparison with producer data and measurements it is evident that analytical model of the motor calculates the motor characteristics with satisfactory accuracy. Accurate calculation of steady state characteristics is only possible if motor parameters are calculated accurately. They are presented in Table 7 and compared with producer data and measurements. The stator winding resistance is the only parameter compared with the measurements because the motor is squirrel cage type and there is no possibility to measure rotor parameters.

Table 7. Motor parameters

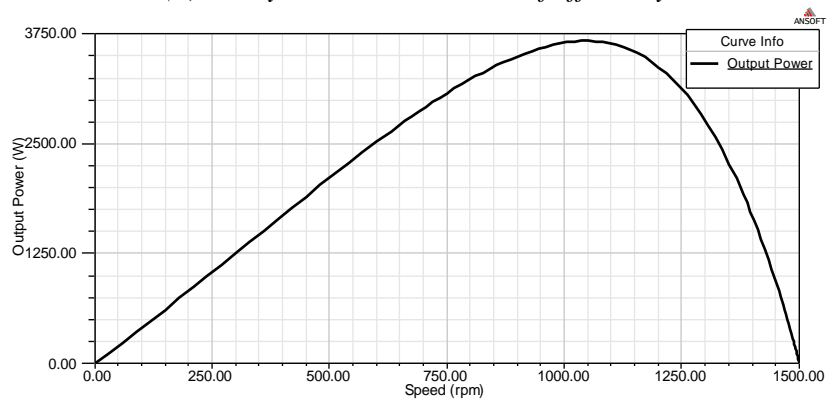
	Analytical model	Producer data	Measurements
Stator resistance at 20 °C (Ω)	2.9	2.76	2.84
Stator leakage reactance (Ω)	3.687	/	/
Rotor resistance at 20 °C (Ω)	3.59	/	/
Rotor leakage reactance (Ω)	3.2	/	/
Magnetizing reactance (Ω)	70.254	/	/



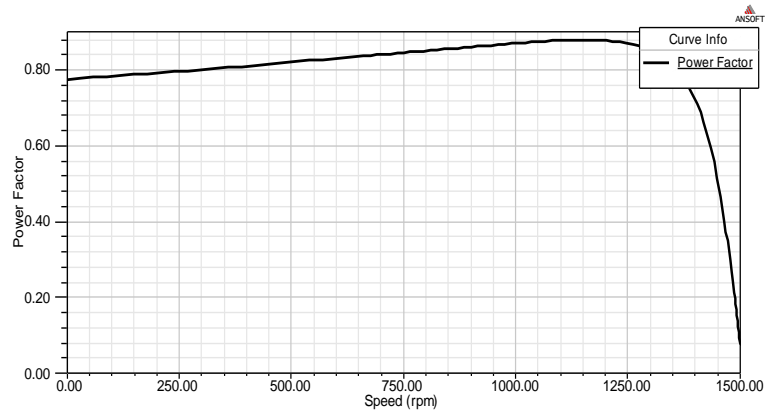
(a) steady-state characteristic of input current



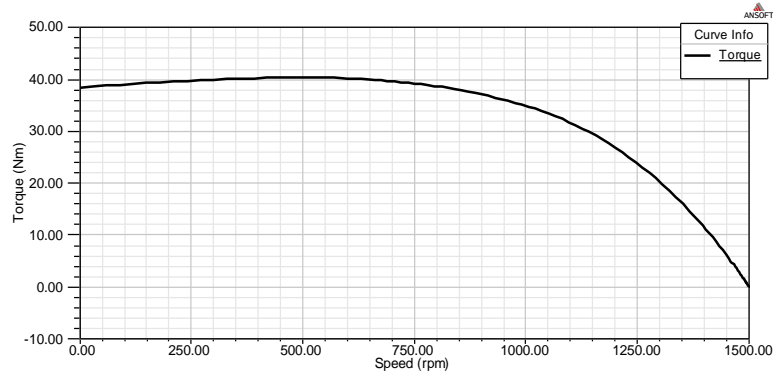
(b) steady-state characteristic of efficiency



(c) steady-state characteristic of output power



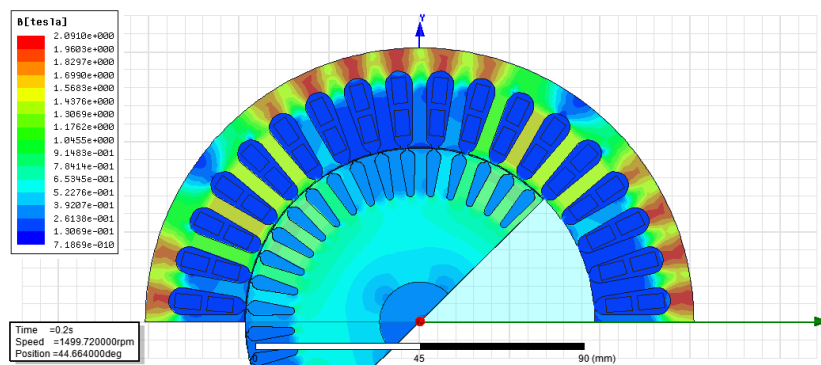
(d) steady-state characteristic of power factor



(e) steady-state characteristic of torque

Figure 5. Steady-state performance characteristics

Numerical model of the motor includes definition of the motor geometry, properties of all materials, boundary conditions on motor outer geometry, type of the excitation and time step for problem solving. Three different numerical models are simulated for three different operating modes: no load (motor speed 1490 rpm), rated operation (motor speed 1362 rpm) and locked rotor (motor speed 0 rpm). For these three modes, magnetic flux density in motor cross section is calculated and transient characteristics of torque. Fig. 6 presents the magnetic flux density in motor cross section for all three mentioned operating modes. From presented results of flux density distribution, it is evident that at no-load and rated load some points of stator yoke have increased flux density, which in case of rated load is close to the point of material saturation. Yet, it can be concluded that the motor design is reasonable as losses and efficiency factor from the analytical model are within the expected ranges for this type of the motor. At locked rotor operation, very small areas of the stator teeth have high flux density. The value of the flux density can be further reduced by applying high quality magnetic materials.



(a) no-load

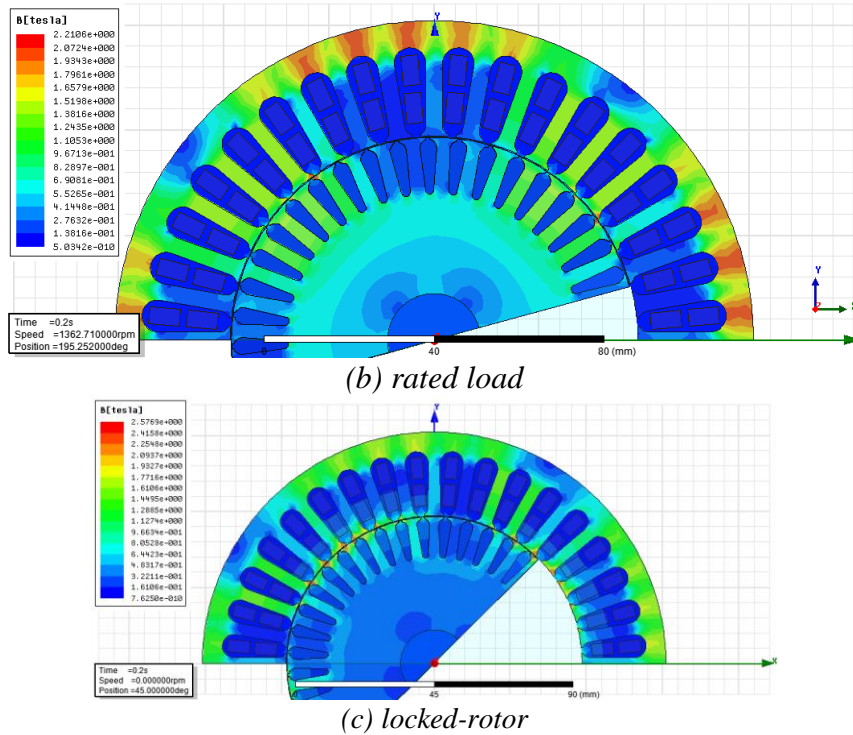


Figure 6. Flux density distribution

Fig. 7 presents the transient characteristics of torque at no-load, rated load and at start-up respectively, obtained from motor numerical model. The numerical model allows obtaining the transient characteristics of torque and calculation of rms values of torque after transients are suppressed. On that way, obtained results of torque can be compared with measurements or with the results from analytical model and steady state characteristics in order to verify the accuracy of the numerical model. Once, the numerical model has been confirmed as accurate enough, the parametric analysis in the numerical model can be run, in order to study the influence of variation of different motor parameters to motor operation i.e. motor output torque. Parametric analysis is a software module in the numerical model (FEM software), which allows influence of different design parameters on the certain target function to be analyzed. Rms values of torque after the motor acceleration has finished, are calculated for each operating mode and they are compared with data from the motor producer and where available with data from measurements. For rated load, motor producer gives 14.9 Nm, from numerical model is 16.1 Nm and from measurements 13.9 Nm [16]. For no-load, from producer data is 1.1 Nm, from numerical model 1.25 Nm and from measurements by taking into consideration that at 1495 rpm (no-load speed), at voltage 220 V, the measured no-load losses are 196 W. According to

equation (20) the no-load torque is 1.25 Nm. For starting torque from producer data it is 33 Nm, from numerical model is 39 Nm [16].

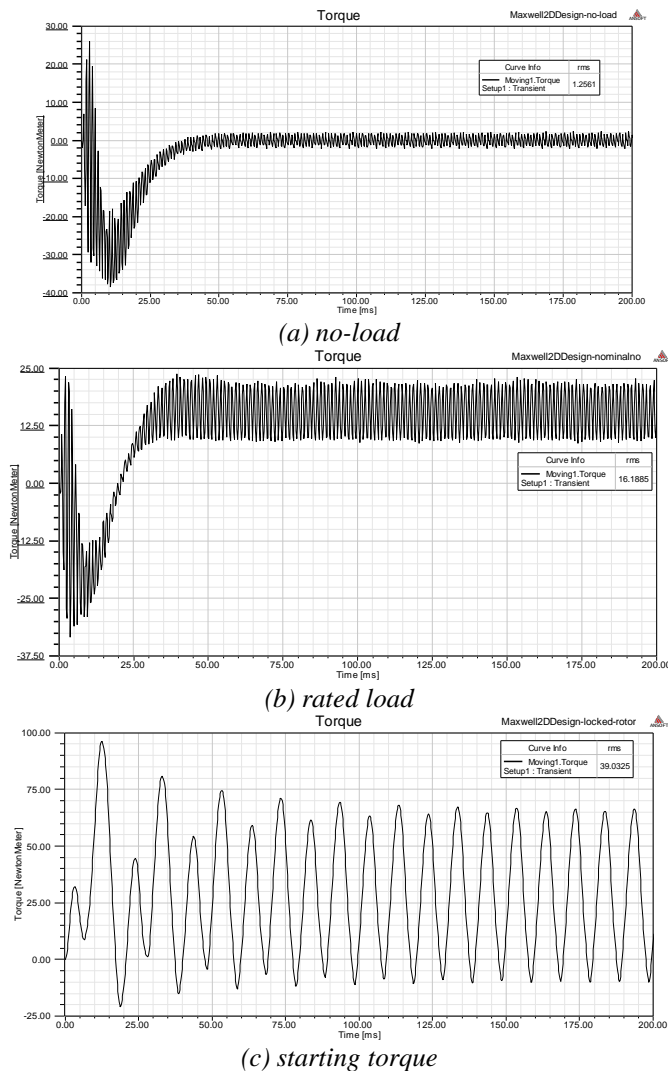


Figure 7. Transient characteristics of torque

Fig. 8 presents the motor torque for different combinations of stator inner diameter and supply voltage. The basic motor model is obtained at voltage magnitude of 310 V, stator inner diameter of 97 mm for which the output torque is 16 Nm (Fig. 7b). As expected, decreased supply voltage reduces the motor torque (Fig. 8). The increased air gap length (increased inner stator diameter) reduces the available torque, increases the magnetizing current, and reduces the power factor. Additional-

ly, motor runs with increased slip. Obtained results from parametric analysis are presented in Table 8.

Table 8. Parametric analysis

Stator inner diameter (mm)	Voltage magnitude (V)	Torque (Nm)
97	300	14.872
97	315	16
97.4	300	14.12
97.4	315	15.22

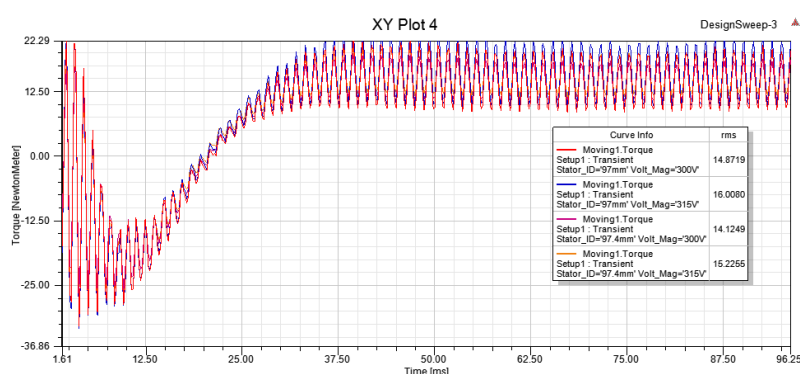


Figure 8. Parametric analysis of torque

From presented results of torque it is evident that analytical and numerical model provide sufficient accuracy for calculating motor torque at steady –state operation and at transient operation. The advantages of presented models are fast computation of the complete motor and its characteristics with few needed input parameters. This reduces the design time for each variant of the same type of the machine allowing the most suitable solution quickly and effectively to be created.

5. CONCLUSION

Paper presents analytical and numerical model of three-phase squirrel cage motor suitable for calculating steady state and transient characteristics at different operating modes. Accuracy of derived models is verified by experiments. Developed analytical model uses few input parameters such us: winding parameters and geometry of core laminations. As an output from this analytical model complete set of motor parameters are calculated and operating characteristics at different speeds are plotted. Numerical model is derived from the analytical. From the numerical model besides steady state and transient characteristics, distribution of the magnetic flux density in motor cross-section is plotted. It allows parts of motor construction with

the high values of flux density to be detected and consequently the motor design to be improved. Parametric analysis is run in the motor numerical model with variation of stator inner diameter and stator voltage. Obtained results confirm that increased length of air gap and reduced stator voltage, reduce the available motor torque. Presented models allow quick changes of motor design with short computing time. This allows a variety of motor designs to be created and the best solution for a given application to be chosen.

REFERENCES

- [1] Ansys. Ansys Maxwell and SGI® UV™ 3000 Maximizes Electromagnetic Computation Throughput., Ansys Inc, 2016.
- [2] Roubache L., Boughrara K., Ibtouen R. Analytical Electromagnetic Analysis of Multi-Phases Cage Rotor Induction Motors in Healthy, Broken Bars and Open phases Conditions, *Progress in Electromagnetics Research B*, (vol. 70), 2016, pp. 113-130.
- [3] Staton D., Popescu M. Analytical Thermal Models for small induction motors. *COMPEL-The international journal for computation and mathematics in electrical and electronic journal*, **5** (vol. 29), 2010, pp. 1345-1360.
- [4] Mirazei M., Mirslaim M., Abdollahi S.E. Analytical Modeling of Axial Air Gap Solid Induction machines using a Quasi-Three-Dimensional Method. *IEEE Transactions on Magnetics*. **7** (vol. 43), 2007, pp. 1-6.
- [5] Qasser L., Puroshothaman S. Closed-Form analysis of Squirrel-Cage Induction Motors With Anisotropic Modeling of Stator and Rotor, *IEEE Transactions on Energy Conversion*, **3** (vol 27), 2012, pp. 553-560.
- [6] Manohran S., Devarajan N., Deivasahayam M.S., Ranganathan G. Review on Efficiency Improvement in Squirrel Cage Induction Motor by Using DCR Technology, *Journal of Electrical Engineering*, **4** (vol.60), 2009, pp. 227-236.
- [7] Ansys, Maxwell 2D User's Guide, Ansys Inc, 2010.
- [8] Vaiman T., Belahcen A., Kallaste A. Changing of Magnetic Flux Density Distribution in a Squirrel-Cage Induction Motor with Broken Rotor Bars, *Elektronika ir Elektrotechnika* **7** (vol.20), 2014, pp. 11-14.
- [9] Ferkova Z. Comparison Between 2D and 3D Modeling of Induction Machine Using Finite Element Method, *Power Engineering and Electrical Engineering*, **2** (vol. 13), 2015, pp. 120-126.
- [10] Griffiths R.D. Automation of finite element aided design of induction motors using multi-slice 2D models, *COMPEL-The international journal for computation*

and mathematics in electrical and electronic journal, **2** (vol. 25), 2006, pp. 309-319.

[11] Martinez J, Belahcen A., Arkiko A. A 2D FEM model for transient and fault analysis of induction machines. *Przeglad Elektrotechniczny* **7b** (vol. 88), 2012, pp. 157-160.

[12] Reljić D., Jerkan D., Marčetić D. Broken Bar Fault Detection in IM Operating Under No-load Condition”, *Advances in Electrical and Computer Engineering*, **4** (vol. 16), 2016, pp. 63-70.

[13] Terzic V.M., Mihic S. D., Vukosavic N S. Stator design and Air Gap Optimization of High Speed Drag-Cup Induction Motor using FEM, *Advances in Electrical and Computer Engineering*, **3** (vol. 13), 2013, pp. 93-100.

[14] E. El-Kharasi, H. M. Hassanien. Reconstruction of the switched-reluctance stator motor, *Journal of Electrical Engineering*, **1** (vol.63), 2012, pp. 2-12.

[15] S. Mihai, A. Simion, L. Livadaru, A. Munteanu, Induction motor with switchable number of poles and toroidal winding, *Advances in Electrical and Computer Engineering*, **2** (vol.11), 2011, pp. 113-118.

[16] Koncar-MES d.d , Three phase squirrel cage induction motor, catalogue

Information about the authors:

Vasilija Sarac- Associate professor at Faculty of Electrical Engineering, University Goce Delcev – Stip. Her main research interests are design, simulation and optimization of electrical machines and power converters.

Dragan Minovski-Associate professor at Faculty of Electrical Engineering, University Goce Delcev – Stip. His main research interests are power engineering and electrical energy conversion.

Peter Janiga- Ing. PhD, employed at Faculty of Electrical Engineering and Information Technology, Slovak University of Technology in Bratislava. His main research interests are power engineering and power quality.

Manuscript received on 15 April 2017

Revised paper received on 13 May 2017